A search for pair-produced resonances in four-jet final states at $\sqrt{s}$ = 13 TeV with the ATLAS detector

The ATLAS Collaboration

A search for massive coloured resonances which are pair produced and each decay into two jets is presented. The analysis uses 36.7 fb^{-1} of pp collision data recorded by the ATLAS experiment at $\sqrt{s}$ = 13 TeV in 2015 and 2016. No significant deviation from the background prediction is observed. Results are interpreted in a SUSY simplified model where the lightest supersymmetric particle is the top squark, $\tilde{t}$, which is pair-produced and decays promptly into two quarks through R-parity violating couplings. Top squarks with masses between $100\,\text{GeV} < m_{\tilde{t}} < 410$ GeV and decaying into two quarks are excluded at 95% confidence level. If the decay is into a b-quark and a light-quark, a dedicated selection requiring at least two b-tags is used to exclude masses between $100\,\text{GeV} < m_{\tilde{t}} < 470$ GeV and $480\,\text{GeV} < m_{\tilde{t}} < 610$ GeV. Additionaly, tight constraints are set on the pair production of massive colour octet resonances.

1 Introduction

Massive coloured particles decaying into quarks and gluons are predicted in several extensions of the Standard Model (SM). At hadron colliders, the search for new phenomena in fully hadronic final states, without missing transverse momentum, is experimentally challenging due to the very large SM multijet production cross-section. This paper describes a search for pair-produced scalar particles each decaying into two jets using 36.7 fb^{-1} of $\sqrt{s} = 13$ TeV proton-proton (pp) collision data recorded in 2015 and 2016 by the ATLAS experiment at the Large Hadron Collider.

Supersymmetry (SUSY) [1–6] is a generalization of the Poincaré symmetry group that fundamentally relates fermionic and bosonic degrees of freedom. In the generic superpotential, Yukawa couplings can lead to baryon- and lepton-number violation:

$$\mathcal{W}_{\text{RPV}} = \kappa_i L_i H_u + \lambda_{ijk} L_i L_j \bar{E}_k + \lambda'_{ijk} L_i \bar{Q}_j \bar{D}_k + \lambda''_{ijk} \bar{U}_i \bar{D}_j \bar{D}_k,$$

where i, j, k are quark and lepton generation indices. The L_i, Q_i represent the lepton and quark $SU(2)_L$ doublet superfields and H_u the Higgs superfield that couples to up-type quarks. The $\bar{E}_i$, $\bar{D}_i$ and $\bar{U}_i$ are the lepton, down-type quark and up-type quark $SU(2)_L$ singlet superfields, respectively. For each term the couplings are given by λ, λ', λ'' and κ is a dimensional mass parameter. The λ and λ'' couplings are antisymmetric in the exchange of $i \to j$ and $j \to k$, respectively. While these terms in many scenarios are removed by imposing an additional Z_2 symmetry (R-parity) [7], the possibility that at least some of these R-parity violating (RPV) couplings are not zero is not ruled out experimentally [8, 9]. This family of models leads to unique collider signatures which would elude conventional searches for R-parity conserving SUSY.

Naturalness arguments [10, 11] suggest higgsinos and top squarks[1] (stops) to be light, with masses below a TeV [12, 13]. Third generation squarks in R-parity conserving scenarios, and top squarks in particular, have been the subject of a thorough programme of searches at the LHC [14–20]. If the top squark decays through RPV operators, however, the existing bounds on its mass can be significantly relaxed. Indirect experimental constraints [21] on the sizes of each of the λ'' couplings from sources other than proton decay are primarily valid for low squark mass and for first- and second-generation couplings.

This search targets a model where the top squark is the lightest supersymmetric particle and decays though baryon-number-violating RPV λ'' couplings, $\tilde{t} \to \bar{q}_j \bar{q}_k$. The couplings are assumed to be not too small, such that the decays are prompt, but small enough to neglect the single top squark resonant production through RPV couplings. Top squarks are then produced through strong interactions with cross-sections that do not depend on the specific assumptions on the SUSY model. For two specific choices of couplings the process considered is schematically depicted in Fig. 1.

In models with extended SUSY, colour octet states can arise as scalar partners of a Dirac gluino [22–25]. These scalar gluons (or sgluons) are dominantly pair-produced, and decay into two quarks or two gluons.

Massive colour octet resonances, generically referred to as colorons (ρ) [26, 27] are predicted in a wide range of other theories, including axigluon [28, 29], Topcolor [30], in vector-like confinement models [31, 32] and as Kaluza-Klein excitations of the gluons [33, 34]. Colorons can be pair produced and decay into two jets, a scenario which leads to a four-jet final state.

---

[1] The superpartners of the left- and right-handed top quarks, $\tilde{t}_L$ and $\tilde{t}_R$, mix to form the two mass eigenstates $\tilde{t}_1$ and $\tilde{t}_2$, where $\tilde{t}_1$ is the lightest one. This analysis considers only the production of the $\tilde{t}_1$, which thereafter is simply refererred to as $\tilde{t}$.

Previous searches for pair produced resonances in hadronic final states have been performed at 7 TeV and 8 TeV by both the ATLAS [35, 36] and CMS experiments [37, 38]. For decays including heavy-flavour jets in the final state, exclusion limits at 95% confidence level (CL) on the mass of the top squark between $100\,\text{GeV} \leq m_{\tilde{t}} \leq 320$ GeV and $200\,\text{GeV} \leq m_{\tilde{t}} \leq 385$ GeV have been reported by ATLAS [36] and CMS [38], respectively. In addition two ATLAS searches [39, 40] have placed constraints on top squarks that decay to $\bar{b}\bar{s}$ when they are produced in the decays of light gluinos.

2 ATLAS detector

The ATLAS detector [41] is a multi-purpose particle physics detector with a forward-backward symmetric cylindrical geometry and nearly 4π coverage in solid angle[2]. The inner tracking detector consists of pixel and silicon microstrip detectors covering the pseudorapidity region $|\eta| < 2.5$, surrounded by a transition radiation tracker which provides electron identification in the region $|\eta| < 2.0$. Starting in Run 2, a new inner pixel layer, the Insertable B-Layer (IBL) [42], has been inserted at a mean sensor radius of 3.3 cm. The inner detector is surrounded by a thin superconducting solenoid providing an axial 2 T magnetic field and by a lead/liquid-argon (LAr) electromagnetic calorimeter covering $|\eta| < 3.2$. A steel/scintillator-tile calorimeter provides hadronic coverage in the central pseudorapidity range ($|\eta| < 1.7$). The endcap and forward regions ($1.5 < |\eta| < 4.9$) of the hadronic calorimeter are made of LAr active layers with either copper or tungsten as the absorber material. An extensive muon spectrometer with an air-core toroid magnet system surrounds the calorimeters. Three layers of high-precision tracking chambers provide coverage in the range $|\eta| < 2.7$, while dedicated fast chambers allow triggering in the region $|\eta| < 2.4$. The ATLAS trigger system consists of a hardware-based level-1 trigger followed by a software-based high level trigger [43].

3 Data Sample

The data used in this analysis were collected by the ATLAS detector in pp collisions at $\sqrt{s} = 13$ TeV at the LHC using a proton bunch crossing interval of 25 ns during 2015 and 2016. In this dataset the mean number of additional pp interactions per proton-bunch crossing (pile-up) is about 23. Events were recorded using a four-jet trigger with transverse momentum (p_T) thresholds of 100 GeV on each jet at the high level trigger which is fully efficient after the analysis selection requirements are applied. After requiring beam, data, and detector quality criteria, the available dataset corresponds to an integrated luminosity of 36.7 fb^{-1} with an associated uncertainty of ±2.1% for the 2015 and ±3.4% for the 2016 data. The uncertainty on the integrated luminosity is obtained from a calibration of the luminosity scale using a pair of beam-separation scans performed in August 2015 and June 2016, following a methodology similar to that detailed in Ref. [44].

---

[2] ATLAS uses a right-handed coordinate system with its origin at the nominal interaction point in the centre of the detector. The positive x-axis is defined by the direction from the interaction point to the centre of the LHC ring, with the positive y-axis pointing upwards, while the beam direction defines the z-axis. Cylindrical coordinates (r, ϕ) are used in the transverse plane, ϕ being the azimuthal angle around the z-axis. The pseudorapidity η is defined in terms of the polar angle θ by $\eta = -\ln\tan(\theta/2)$. Rapidity is defined as $y = 0.5 \cdot \ln[(E + p_z)/(E - p_z)]$ where E denotes the energy and p_z is the component of the momentum along the beam direction.

4 Simulated samples

The dominant background of SM multijet production is estimated with a data-driven technique, while Monte Carlo (MC) simulated events are used to estimate the contribution of the $t\bar{t}$ background, to model the signals and to establish and validate the background estimation method.

The response of the detector is simulated [45] either using a GEANT4 simulation [46] or by a fast parametrised simulation [47] of the calorimeter response and GEANT4 for everything else. To account for pile-up interactions in the same and close-by bunch crossings (pileup), a set of minimum bias interactions is generated using PYTHIA 8.186 [48] with the A2 set of parameters [49] and the MSTW2008LO [50, 51] parton density function (PDF) set and is superimposed on the hard scattering events. The EvtGen v1.2.0 program [52] is used to simulate properties of bottom and charm hadron decays for all samples. Corrections are applied to the simulated events to account for differences between data and simulation for the efficiency of identifying jets originating from the fragmentation of b-quarks, together with the probability for mis-tagging light-flavour and charm quarks.

Background samples of multijet production are simulated with $2 \rightarrow 2$ matrix elements (ME) at leading order (LO) using the PYTHIA 8.186 generator. The renormalisation and factorisation scales are set to the average p_{T} of the two leading jets. The ATLAS A14 set [53] of parton shower and multiple parton interaction parameters (tune) is used together with the NNPDF23LO PDF set [54].

Top pair production events are simulated using the POWHEG-BOX v2 [55] generator with the CT10 PDF set. The top mass is set to 172.5 GeV. The h_{damp} parameter, which regulates the p_{T} of the first extra emission beyond the Born configuration (and thus controls the p_{T} of the $t\bar{t}$ system) is set to the mass of the top quark. The parton shower, fragmentation, and underlying event are simulated using PYTHIA 6.428 [56] with the CTEQ6L1 PDF set and the corresponding Perugia 2012 tune (P2012) [57]. The sample is normalised to the next-to-next-to-leading order (NNLO) cross-section including the resummation of soft gluon emission at next-to-next-to-logarithmic (NNLL) accuracy using `Top++2.0` [58].

The search considers three benchmark signals: the pair production of top squarks, colorons and sgluons with decays into four jets. Signal samples are generated using MG5_aMC@NLO [59] v2.2.3 interfaced to PYTHIA 8.186 with the A14 tune for the modeling of the parton shower, hadronization and underlying event. The ME calculation is performed at leading order and, for the top squark signal, includes the emission of up to two additional partons. The matching with the parton shower is done using the CKKW-L [60] prescription, with a matching scale set to one quarter of the pair-produced resonance mass. The PDF set used for the generation is NNPDF23LO. For the top squark signal generation all the non-SM particle masses are set to 5 TeV except for the top squark ($m_{\tilde{t}}$). The top squark is decayed in PYTHIA 8 assuming a 100% branching ratio into $\bar{b}\bar{s}$. Its width is expected to be small, and negligible with respect to the detector resolution. The top squark pair-production cross-sections are calculated at next-to-leading order (NLO) in the strong coupling constant, adding the resummation of soft gluon emission at next-to-leading-logarithmic accuracy [61–63]. The nominal cross-section and its uncertainty are taken from an envelope of cross-section predictions using different PDF sets and factorisation and renormalisation scales, as described in Ref. [64]. The coloron samples are generated with the model described in Ref. [65], where the couplings of the vector colour octet to all particles except to light-quarks are set to zero. The LO cross-sections from the generator are used. The coloron samples are also used to set an interpretation for sgluon pair-production, where they are scaled to the sgluon cross-section computed at NLO with MG5_aMC@NLO [66, 67]. The sgluons are assumed to decay into two gluons, which in this analysis are not distinguished from quark-jets.
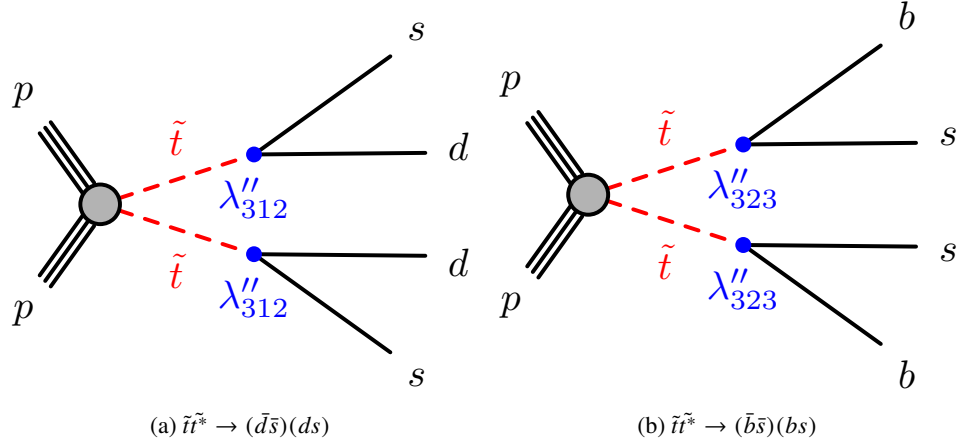
4

(a) $\tilde{t}\tilde{t}^* \to (\bar{d}\bar{s})(ds)$ (b) $\tilde{t}\tilde{t}^* \to (\bar{b}\bar{s})(bs)$

Figure 1: Diagrams depicting the direct pair-production of top squarks through strong interactions, with decays into a d- and an s-quarks (left) or to a b- and an s-quark (right) through the λ'' R-parity violating couplings, indicated by the blue dots.

5 Object reconstruction

Candidate jets are reconstructed from three-dimensional topological energy clusters [68] in the calorimeter using the anti-k_t jet algorithm [69] with a radius parameter of 0.4. Each topological cluster is calibrated to the electromagnetic scale response prior to jet reconstruction. The reconstructed jets are then calibrated to the particle level by the application of a jet energy scale (JES) calibration derived from simulation and in situ corrections based on 13 TeV data [70–72]. The `TightBad` cleaning quality criteria [73] are imposed to identify jets arising from non-collision sources or detector noise. Any event containing at least one jet failing quality requirements with $p_T > 20$ GeV is removed.

Jets containing b-hadrons (b-jets) are tagged by a multivariate algorithm (MV2c10) using information about the impact parameters of inner detector tracks associated to the jet, the presence of displaced secondary vertices, and the reconstructed flight paths of b- and c-hadrons inside the jet [74]. A working point with a 77% efficiency, as determined in a simulated sample of $t\bar{t}$ events, was chosen. The corresponding rejection factors against jets originating from c-quarks and from light-quarks or gluons are 4.5 and 130, respectively [75].

6 Event Selection

Each event is required to have a reconstructed primary vertex consistent in location with the beamspot envelope, with at least two associated tracks with $p_T > 400$ MeV. If more than one such vertex is found, the vertex with the largest $\sum p_T^2$ of the associated tracks is chosen.

The final state under consideration consists of four jets forming two pairs, originating from a pair of equal mass resonances. After the trigger requirement, only events with at least four reconstructed jets with $p_T > 120$ GeV and $|\eta| < 2.4$ are retained in the analysis.

The analysis strategy exploits the case where the resonances are produced with a significant transverse momentum. As a result the decay products are expected to be close-by. Taking advantage of this property, candidate resonances are constructed by pairing the four leading jets in the event. Two jet pairs are identified by minimizing the following quantity:

$$\Delta R_{\mathrm{min}} = \sum_{i=1,2} |\Delta R_i - 1|$$

where ΔR_i is the angular distance between the two jets for the ith pair and the sum is over the two pairs of dijets. The offset of -1 has been chosen to maximise the signal efficiency for the masses of interest while minimizing the effects of soft jets from radiated gluons being recombined with their parent jets in multijet topologies.

The above criteria define the analysis preselection. Additional selections are applied to further enhance the signal fraction. These are based on four discriminating variables established from simulation studies and previous ATLAS searches [32, 35, 36].

To reduce the non-resonant multijet background, where the efficiency of the pairing is expected to be poor, a quality criterion is applied on the pairing metric. Resonances of larger masses are produced with a lower boost, and their decay products are less collimated. To compensate for the larger (smaller) angular separation between the jets at high mass (low mass) this requirement is made dependent on the average mass of the two resonance candidates in the event, m_{avg}. The event is discarded if the best combination of the four leading jets satisfies:

$$\Delta R_{\mathrm{min}} > -0.002 \cdot (m_{\mathrm{avg}}/\mathrm{GeV} - 225) + 0.72 \qquad \text{if } m_{\mathrm{avg}} \leq 225 \text{ GeV}$$
$$\Delta R_{\mathrm{min}} > +0.0013 \cdot (m_{\mathrm{avg}}/\mathrm{GeV} - 225) + 0.72 \qquad \text{if } m_{\mathrm{avg}} > 225 \text{ GeV}.$$

After boosting the system formed by the two resonances into its centre-of-mass frame, the cosine of the angle that either of them forms with the beamline is defined as $|\cos(\theta^*)|$. Background jets from multijet production are frequently originating from t-channel gluon exchange and are preferentially produced in the forward region, with $|\cos(\theta^*)|$ close to one. Jets originating from the signal are instead expected to be more central and lead to small $|\cos(\theta^*)|$ values.

Since the two reconstructed resonances are expected to have equal mass, their mass difference is a powerful discriminant between signal and background. The mass asymmetry ($\mathcal{A}$) is defined as:

$$\mathcal{A} = \frac{|m_1 - m_2|}{m_1 + m_2} \, .$$

where m_1 and m_2 are the invariant masses of the two reconstructed dijet pairs. $\mathcal{A}$ is expected to be close to zero for well-paired signal events and is relatively constant for background events.

The distributions of ΔR_{min}, $\mathcal{A}$ and $|\cos(\theta^*)|$ at preselection are shown for data, a top squark sample with a mass of $m_{\tilde{t}} = 500$ GeV and a coloron sample with mass $m_\rho = 1250$ GeV in Fig. 2. Given the very small signal purity expected before additional selections are applied, the data distribution can be viewed as representative of the background expectation. Two additional requirements, of $\mathcal{A} < 0.05$ and $|\cos(\theta^*)| < 0.3$, define the inclusive signal region (SR), targeting resonance decays into light-quark or gluons jets. The selections have been determined in an optimisation procedure that maximises the expected signal significance.
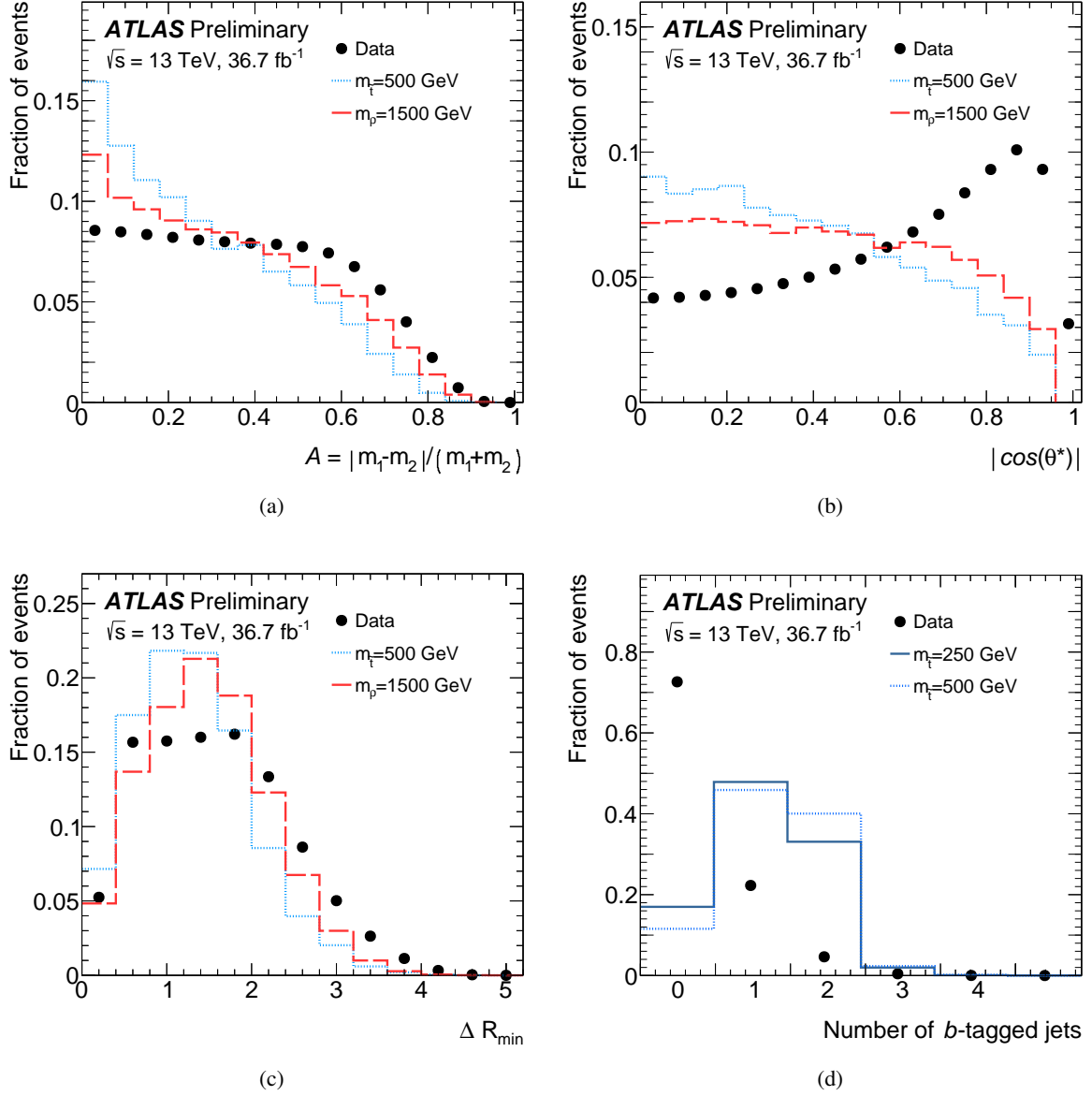
Figure 2: The distributions of the (a) mass asymmetry ($\mathcal{A}$), the (b) stop pair production angle $|\cos(\theta^*)|$, the (c) smallest angular separation between the two jets in a pair ($\Delta R_{\min}$) and the (d) multiplicity of b-tagged jets. The distributions are shown after pairing the four jets into resonance candidates, before any additional requirement is applied. The observed data (black dots) are compared with the distributions expected from a top squark with a mass of 250 GeV (open blue crosses) or 500 GeV (open blue triangles) and a coloron with a mass of 1.25 TeV (open red squares). The distributions are normalised to unity and shown after the requirement of four jets paired into two candidate resonances.
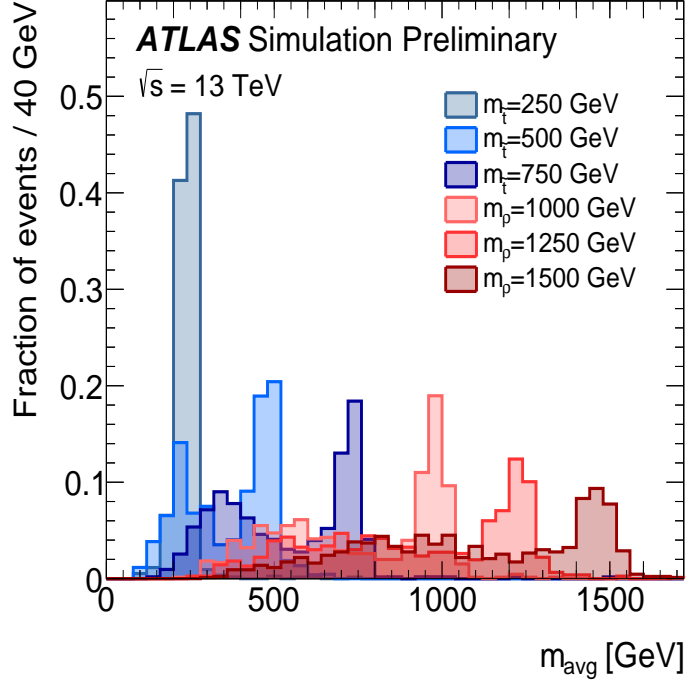
Figure 3: Distribution of the average mass, m_{avg}, in the inclusive signal region for top squark signals with $m_{\tilde{t}}$ = 250 GeV, 500 GeV, 750 GeV and coloron signals with m_{ρ} = 1.0 TeV, 1.25 TeV, 1.5 TeV.

If RPV couplings involving third generation quarks, λ''_{3i3}, dominate a b-quark is expected from each of the top squark decays. A dedicated b-tagged SR selection is used for this scenario. On top of the requirements applied in the inclusive selection it requires at least two b-tagged jets to be present in the event, which significantly reduces the multijet background. The distribution of the number of b-tagged jets after pairing the four jets into candidate resonances is shown for data and two top squark signals with masses of 250 and 500 GeV in Fig. 2d. An additional factor of about two in background reduction is gained by imposing that each of the two b-jets is associated with a different reconstructed resonance. This is particularly effective in reducing the contribution of $g \rightarrow b\bar{b}$ splittings, where the two b-jets are typically very collimated.

The final analysis discriminant is the average mass of the two reconstructed resonances:

$$m_{avg} = \frac{1}{2}(m_1 + m_2)$$

A peak in m_{avg} at a mass of about that of the resonance is expected for the signal, over a non-peaking background from multijet processes. Figure 3 shows the expected m_{avg} distribution for signal samples with different masses. For each mass hypothesis a counting experiment is performed in a window of the m_{avg} variable optimised to maximise the expected signal significance. The windows range from a 10 GeV width for a 100 GeV top squark to a 200 GeV width for a 1.5 TeV coloron. The mass window for the highest target mass of 2 TeV considered has no upper edge. For signals closer in mass than the experimental resolution, the related mass windows partially overlap.

The expected event yields in simulation in 36.7 fb^{-1} are shown in Table 1 after each different requirement is applied. The acceptance times efficiency of the inclusive and b-tagged selections as a function of
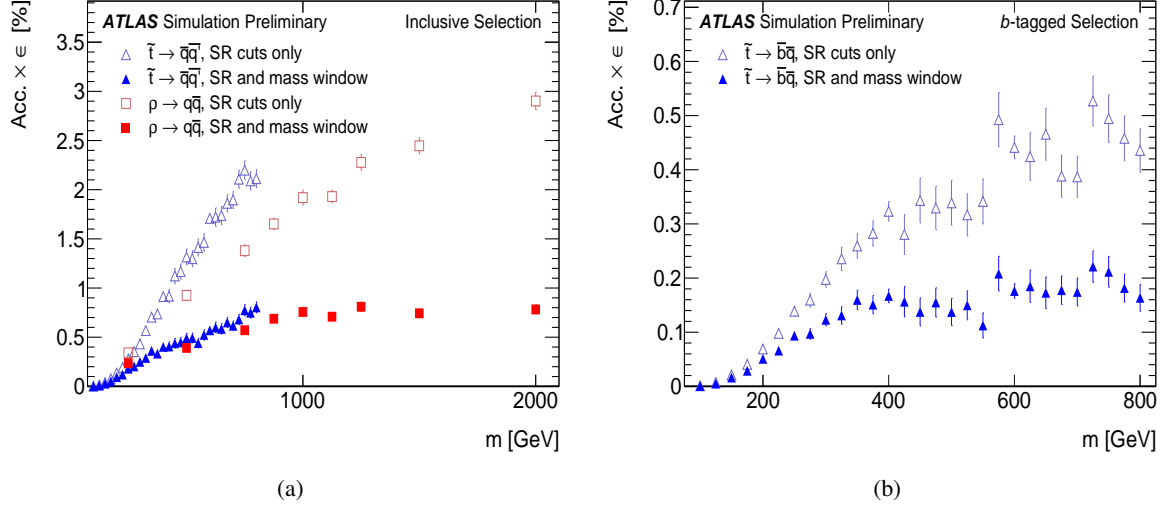
Figure 4: The acceptance times efficiency (Acc.×ϵ) of the inclusive (a) and b-tagged (b) signal region selection is shown as a function of the resonance mass, m, before and after the mass window requirements are applied. Top squark signals are indicated by the blue triangles, coloron by the red squares. The statistical uncertainties are indicated by vertical bars.

Table 1: The expected number of signal events in 36.7 fb^{-1} from MC simulation for each of the selections applied. Top squark masses of $m_{\tilde{t}}$ = 100 GeV and $m_{\tilde{t}}$ = 500 GeV and a coloron mass of 1.5 TeV are shown. The statistical uncertainty of the MC simulation is shown for each selection.

Selection	$m_{\tilde{t}}$ = 100 GeV	$m_{\tilde{t}}$ = 500 GeV	m_{ρ} = 1500 GeV
Total	613100 ± 700	18400 ± 130	1710 ± 10
Trigger	221900 ± 420	11900 ± 100	1650 ± 10
$\Delta R_{\min}$	18910 ± 120	2470 ± 50	1050 ± 5
Inclusive selection	1359 ± 36	253 ± 16	51 ± 2
b-tagged selection	569 ± 24	65 ± 8	–

9

the signal mass are shown before and after applying the m_{avg} mass window requirement in Fig. 4. The acceptance of the SR selections increases for large masses due to the four jets from the signal having a larger p_{T}. However, as the jet pairing does not always correctly assign the resonance candidates for high masses, the signal has a tail extending to low m_{avg} values, degrading the efficiency of the mass window selection.

7 Background estimation

The dominant background from multijet production is estimated directly from data, with a method that predicts both the normalisation and the shape of the m_{avg} distribution. In the b-tagged selection, for m_{avg} below 200 GeV, the $t\bar{t}$ contribution becomes significant, and is estimated from simulation.

For the inclusive selection the m_{avg} distribution in the signal region is obtained from data. For each m_{avg} bin the data sample is divided into one region where the signal selection is applied (D) and three background dominated control regions (A, C and F). The variables used to define the different regions, summarised in Fig. 5, are $\mathcal{A}$ and $|\cos(\theta^*)|$. Provided the two variables defining the regions are uncorrelated, and the signal leakage in the background dominated regions can be neglected, the amount of background in the region of interest D can be predicted from the observed number of events in the control regions as $N_D = N_A \times N_F / N_C$. Two additional regions are defined in the $\mathcal{A}$-$|\cos(\theta^*)|$ plane. They define a validation region (VR), region E, which is used to test the performance of the data driven method and assign an uncertainty to the background estimate. The validation region is defined with the same selections of the signal region, with the asymmetry requirement changed to $0.05 < \mathcal{A} < 0.15$. The background contribution in the VR is estimated as $N_E = N_B \times N_F / N_C$. In the inclusive selection the data-driven estimate also accounts for the contribution from the $t\bar{t}$ production, which amounts to less than 1% of the total background for $m_{\mathrm{avg}} < 200$ GeV, and is negligible above. The linear correlation between the $|\cos(\theta^*)|$ and $\mathcal{A}$ variables has been evaluated in data and simulated multijet samples, where it amounts to 1.8% and 2.2%, respectively. To reduce the impact of correlations observed in data at large m_{avg} and high $\mathcal{A}$ values the $\mathcal{A}$-$|\cos(\theta^*)|$ plane is restricted to $0.0 < \mathcal{A} < 0.7$ and $0.0 < |\cos(\theta^*)| < 0.7$.

For the b-tagged selection the large amount of signal contamination present in region A would potentially bias the result of the background estimate. The multijet background for this selection is thus estimated in two steps. The shape of the m_{avg} distribution is first predicted in a region with a b-tag veto (zero-tag) and then extrapolated to the b-tagged signal region. The m_{avg} distribution in the zero-tag region is obtained with a data-driven estimate, analogously to the inclusive selection. The zero-tag prediction is then extrapolated to the two b-tag plane by means of projection factors computed bin-by-bin in m_{avg}, similarly to the approach described in Ref. [36]. The projection factors, for a given m_{avg} bin and region X, are defined as the ratio between the number of events in the two-tag over the zero-tag planes (N_{X2}/N_{X0}). To avoid being sensitive to signal contamination the projection factor is evaluated in region F. The contributions from multi-jet and $t\bar{t}$ production have different scaling going from the zero- to the b-tagged selection. Hence, simulated samples are used to subtract the $t\bar{t}$ contribution in all control regions. The $t\bar{t}$ estimate in the signal region is then obtained directly from the simulation, considering all relevant modeling and experimental uncertainties.

The observed number of events in each of the regions used in the background estimate of both the inclusive and b-tagged selections is shown before applying the mass window requirements in Table 2. Within the statistical uncertainties the method is seen to well reproduce both the normalisation and the shape of m_{avg} in the VRs. The agreement observed in the VRs is used to derive a systematic uncertainty on the
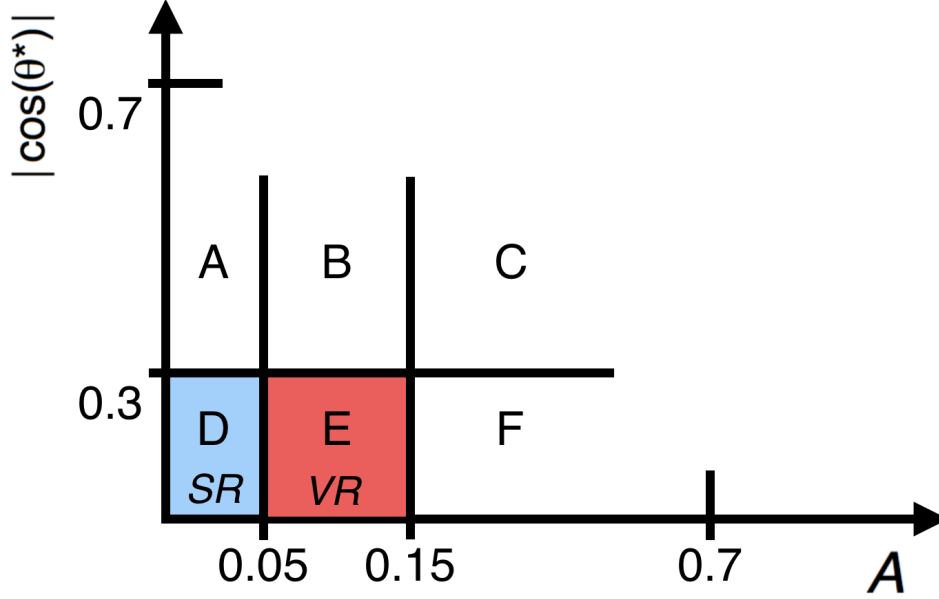
Figure 5: Scheme of the control regions in the $|\cos(\theta^*)|$ and $\mathcal{A}$ plane defined to estimate the multijet background and to obtain the related uncertainty.

background estimate in the SR. In each m_{avg} mass window the difference between the observed data and the prediction in the VR (non-closure) is computed. The largest between the observed non-closure in the VR and the statistical uncertainty of the data-driven method is assigned as uncertainty on the background estimate. To obtain a monotonically increasing uncertainty as a function of mass, and avoid to quote an unphysically small value of the systematic uncertainty for the mass windows where it crosses sign, this uncertainty is further smoothed as a function of m_{avg}. The Nadaraya-Watson [76, 77] kernel regression estimate is used for the smoothing, with a bandwidth of 500 GeV (meaning that the quartiles of the kernels are placed at ±125 GeV). The uncertainties assigned on the background prediction in the inclusive and b-tagged selections are summarised in Fig. 6.

8 Systematic Uncertainties

While the multijet background uncertainties pertain primarily to the estimation method itself, the top background and the signals are also affected by uncertainties related to the description of detector effects and to the physics modelling of the MC simulation.

The dominant detector-related systematic effects are due to the uncertainties on the jet energy scale (JES) [72] and resolution (JER) [78] and from the b-tagging efficiency and mistag rate [75].

Since MC simulation is used to determine the contribution from top events in the b-tagged signal region, systematic uncertainties related to the MC generator of the process need to be estimated. These are evaluated by comparing the nominal samples to additional samples with systematic variations. A modelling uncertainty is derived by comparing the predictions of the nominal sample with a sample produced with Powheg interfaced with Herwig++ 2.7.1, or with MG5_aMC@NLO and showered with Herwig++. In
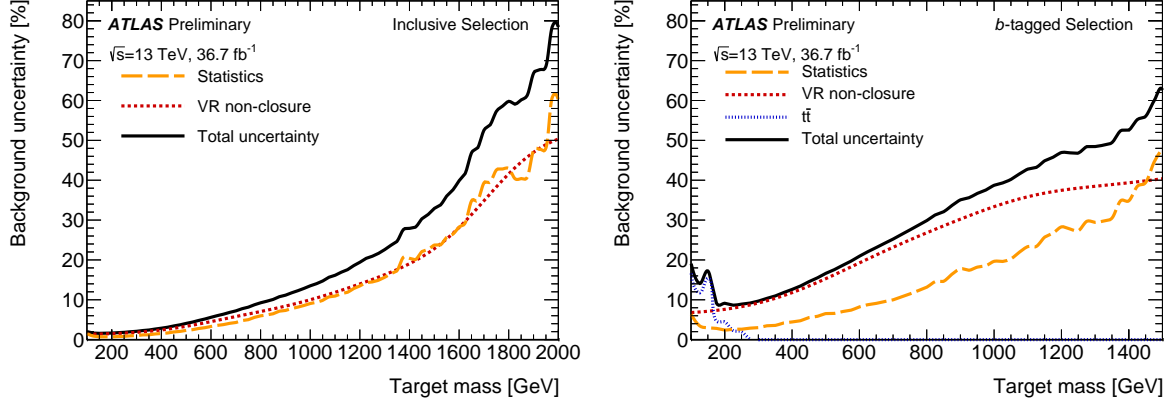
Figure 6: The uncertainty on the data-driven background estimate in the signal regions, computed in the m_{avg} mass windows defined for different target masses, and shown for the inclusive (left) and b-tagged (right) selections. The uncertainty arising from the non-closure in the validation region is shown with a red dashed line and compared with the statistical uncertainty of the data-driven prediction shown as an orange dashed line. The additional uncertainty on the MC estimate of the top background in the b-tagged region is shown as a dotted blue line. The total uncertainty, obtained by adding in quadrature the different components, is indicated by a black solid line.

addition the difference in the prediction obtained by modifying the parton-shower intensity and the h_{damp} parameter in the nominal sample is taken as uncertainty. The size of the total $t\bar{t}$ systematic uncertainty is up to 40% for m_{avg} below 200 GeV, while above 200 GeV the $t\bar{t}$ background contribution becomes negligible.

The total detector related uncertainties on the signal amount to about 10% for the inclusive selection and to about 15% for the b-tagged selection. For top squark production the nominal signal cross-sections and their uncertainties are taken from an envelope of cross-section predictions derived using different PDF sets and different factorisation and renormalisation scales, as described in Ref. [64]. The theoretical uncertainties on the acceptance of the signal simulation include variations of the renormalisation and factorisation scales, the CKKW-L merging scales, and the value of the strong coupling constant in MG5_aMC@NLO as well as parton shower uncertainties in PYTHIA 8 evaluated from variations of the A14 parameters set. After normalising the samples to the same cross-section, the difference in the yield in the mass window, which is typically below 1%, is considered as an uncertainty.

9 Results and interpretation

The m_{avg} distribution in the inclusive and b-tagged signal region selections are shown in Fig. 7. Agreement is observed between data and the expected background. The expected number of background and signal events in the SR and their uncertainties are reported for the mass windows defined for top squark and coloron signals in Tables 3 and 4, respectively. Table 5 presents the numbers in the top squark mass windows of the b-tagged selection.

To estimate the compatibility of data with a generic resonance mass hypothesis, the m_{avg} distribution is scanned in 12.5 GeV steps. The m_{avg} window for an arbitrary mass is obtained from a linear fit to the lower and upper edges of the windows obtained for the simulated signal masses. For each mass an SM background p_0-value is computed, as shown in Fig. 8 for the inclusive (left) and b-tagged selections

Table 2: The observed number of events and the predicted $t\bar{t}$ contribution in each of the regions used in the background estimate, for each b-tag multiplicity. The expected fractional signal contributions are shown for the mass windows corresponding to $m_{\tilde{t}} = 125$ GeV, 250 GeV, 500 GeV, and 800 GeV. For the $m_{\tilde{t}} = 125$ GeV, 250 GeV mass windows the fractions of $t\bar{t}$ are also shown. The $t\bar{t}$ systematic uncertainties include both the detector-level uncertainties and the theoretical uncertainties, as described in Section 8.

Region	N_data	$N_{t\bar{t}}$ ($\pm$ stat. $\pm$ syst.)	[120, 135]GeV $\frac{N_\text{Sig}}{N_\text{Data}}$	$\frac{N_{t\bar{t}}}{N_\text{Data}}$	[230, 260]GeV $\frac{N_\text{Sig}}{N_\text{Data}}$	$\frac{N_{t\bar{t}}}{N_\text{Data}}$	[455, 515]GeV $\frac{N_\text{Sig}}{N_\text{Data}}$	[720, 820]GeV $\frac{N_\text{Sig}}{N_\text{Data}}$
			Inclusive selection					
A	256 937	5 044 $\pm$ 76 $\pm$ 1 100	7.2 %	5.8 %	5.6 %	0.28 %	3.1 %	1.7 %
B	508 589	8 900 $\pm$ 100 $\pm$ 1 400	1.95 %	4.7 %	1.3 %	0.24 %	0.6 %	0.4 %
C	1 154 721	13 080 $\pm$ 120 $\pm$ 2 000	0.17 %	2.3 %	0.16 %	0.43 %	0.07 %	0.07 %
D (SR)	154 750	3 826 $\pm$ 66 $\pm$ 810	14.0 %	7.0 %	10.5 %	0.31 %	6.3 %	3.5 %
E (VR)	307 268	6 578 $\pm$ 87 $\pm$ 1 000	3.86 %	6.0 %	2.2 %	0.33 %	1.4 %	0.8 %
F	694 492	9 920 $\pm$ 110 $\pm$ 1 900	0.29 %	3.5 %	0.3 %	0.57 %	0.2 %	0.13 %
			Zero-tag selection					
A	184 432	580 $\pm$ 27 $\pm$ 85	0.56 %	0.53 %	0.44 %	0.11 %	0.50 %	0.46 %
B	366 003	1 165 $\pm$ 38 $\pm$ 210	0.14 %	0.57 %	0.18 %	0.10 %	0.12 %	0.19 %
C	834 944	2 352 $\pm$ 53 $\pm$ 400	0.07 %	0.66 %	0.03 %	0.13 %	0.02 %	0.04 %
D	110 071	506 $\pm$ 26 $\pm$ 94	1.18 %	0.72 %	1.65 %	0.16 %	1.48 %	1.3 %
E	219 366	831 $\pm$ 32 $\pm$ 180	0.45 %	0.67 %	0.24 %	0.11 %	0.10 %	0.4 %
F	498 751	1 743 $\pm$ 46 $\pm$ 290	0.07 %	0.83 %	0.08 %	0.20 %	0.08 %	0.04 %
			b-tagged selection					
A	8 484	2 375 $\pm$ 53 $\pm$ 900	82 %	64 %	12 %	0.94 %	43 %	18.2 %
B	16 113	3 614 $\pm$ 64 $\pm$ 870	23 %	53 %	23 %	1.4 %	11 %	4.5 %
C	32 759	3 681 $\pm$ 63 $\pm$ 840	1.2 %	31 %	1.3 %	2.2 %	0.38 %	0.1 %
D (SR)	5 603	1 707 $\pm$ 44 $\pm$ 500	135 %	64 %	181 %	0.54 %	70 %	24.6 %
E (VR)	10 531	2 678 $\pm$ 55 $\pm$ 500	38 %	58 %	35 %	0.9 %	20 %	9.2 %
F	20 856	2 904 $\pm$ 56 $\pm$ 720	2.3 %	37 %	31 %	2.7 %	1.4 %	0.7 %

(right). The largest deviation is found in the b-tagged selection for a mass of 463 GeV, corresponding to a p_0-value of 0.005.

The expected p_0-values in each mass window are also evaluated for potential signals. A three sigma signal sensitivity is expected for top squark masses up to 350 GeV with the inclusive selection and 450 GeV with the b-tagged selection. For colorons a three sigma sensitivity is expected for masses up to 1.4 TeV.

In the absence of a statistically significant excess in data, exclusion limits can be derived on the signal models of interest. The inclusive selection is used to set a limit on top squark, sgluon and coloron production with decays into pair of jets, while the two-tag selection is used to interpret the search for top squark pair production with decays into a b- and a light-jet. A profile likelihood ratio combining Poisson probabilities for signal and background is computed to determine the 95% CL for compatibility of the data with the signal-plus-background hypothesis (CL_{s+b}) [79]. A similar calculation is performed for the background-only hypothesis (CL_b). From the ratio of these two quantities, the confidence level for the presence of a signal (CL_s) is determined [80]. Systematic uncertainties are treated as nuisance parameters and are assumed to follow Gaussian distributions. The results are evaluated using pseudo-experiments. This procedure is implemented using a software framework for statistical data analysis, HistFitter [81].

Table 3: The observed number of events in the data, N_{Data}, the estimated number of background, N_{Bkg}, and expected signal, N_{Sig}, events with their statistical and systematic uncertainties computed in the top squark mass windows of the inclusive selection.

$m_{\tilde{t}}$ [GeV]	Window [GeV]	N_{Data}	N_{Bkg} ($\pm$ stat. $\pm$ syst.)			N_{Sig} ($\pm$ stat. $\pm$ syst.)		
100	[100, 110]	5899	5 910	$\pm$ 90	$\pm$ 70	519	$\pm$23	$\pm$ 68
125	[120, 135]	13497	13 450	$\pm$120	$\pm$180	1 890	$\pm$50	$\pm$190
150	[140, 160]	18609	18 390	$\pm$130	$\pm$250	2 540	$\pm$50	$\pm$130
175	[165, 185]	17742	17 800	$\pm$130	$\pm$250	2 280	$\pm$50	$\pm$210
200	[185, 210]	19844	19 660	$\pm$140	$\pm$290	2 250	$\pm$50	$\pm$170
225	[210, 235]	14898	15 180	$\pm$120	$\pm$230	1 620	$\pm$40	$\pm$100
250	[230, 260]	13689	13 750	$\pm$110	$\pm$220	1 440	$\pm$80	$\pm$140
275	[255, 285]	9808	9 860	$\pm$ 10	$\pm$ 70	1 010	$\pm$70	$\pm$ 80
300	[275, 310]	8514	8 790	$\pm$ 90	$\pm$ 60	789	$\pm$52	$\pm$ 31
325	[300, 335]	6180	6 330	$\pm$ 80	$\pm$ 20	600	$\pm$50	$\pm$ 50
350	[320, 365]	5802	5 900	$\pm$ 70	$\pm$ 20	509	$\pm$39	$\pm$ 19
375	[345, 390]	4113	4 250	$\pm$ 60	$\pm$ 90	324	$\pm$25	$\pm$ 31
400	[365, 415]	3531	3 590	$\pm$ 60	$\pm$ 90	274	$\pm$14	$\pm$ 18
425	[385, 440]	3108	3 010	$\pm$ 50	$\pm$ 80	198	$\pm$23	$\pm$ 1
450	[410, 465]	2281	2 230	$\pm$ 40	$\pm$ 60	154	$\pm$17	$\pm$ 27
475	[430, 490]	1906	1 920	$\pm$ 40	$\pm$ 60	116	$\pm$12	$\pm$ 8
500	[455, 515]	1495	1 513	$\pm$ 35	$\pm$ 49	94	$\pm$10	$\pm$ 8
525	[475, 540]	1318	1 327	$\pm$ 33	$\pm$ 46	71	$\pm$ 7	$\pm$ 4
550	[500, 565]	1050	1 048	$\pm$ 29	$\pm$ 39	48.5	$\pm$ 5.4	$\pm$ 2.2
575	[520, 590]	924	912	$\pm$ 27	$\pm$ 36	44	$\pm$ 4	$\pm$ 4
600	[545, 620]	745	744	$\pm$ 25	$\pm$ 31	36.9	$\pm$ 1.6	$\pm$ 2.3
625	[565, 645]	645	626	$\pm$ 22	$\pm$ 28	30.3	$\pm$ 2.8	$\pm$ 3.4
650	[585, 670]	536	554	$\pm$ 21	$\pm$ 26	23.3	$\pm$ 2.1	$\pm$ 1.9
675	[610, 695]	438	473	$\pm$ 19	$\pm$ 24	20.3	$\pm$ 1.6	$\pm$ 0.9
700	[630, 720]	404	422	$\pm$ 18	$\pm$ 22	15.4	$\pm$ 1.2	$\pm$ 0.9
725	[655, 745]	341	335	$\pm$ 16	$\pm$ 18	13.6	$\pm$ 1.0	$\pm$ 0.9
750	[675, 770]	306	310	$\pm$ 16	$\pm$ 18	12.4	$\pm$ 0.9	$\pm$ 0.9
775	[700, 795]	265	243	$\pm$ 14	$\pm$ 14	9.7	$\pm$ 0.7	$\pm$ 0.7
800	[720, 820]	238	205	$\pm$ 12	$\pm$ 13	8.5	$\pm$ 0.6	$\pm$ 0.6

Table 4: The observed number of events in the data, N_{Data}, the estimated number of background, N_{Bkg}, and signal, N_{Sig}, events with their statistical and systematic uncertainties computed in the coloron mass windows of the inclusive selection.

| m_{ρ} [GeV]	Window [GeV]	N_{Data}	N_{Bkg} ($\pm$ stat. $\pm$ syst.)			N_{Sig} ($\pm$ stat. $\pm$ syst.)		
500	[455, 515]	1495	1 513	$\pm$35	$\pm$15	23 000	$\pm$1 900	$\pm$1 200
625	[565, 645]	645	626	$\pm$22	$\pm$35	7 050	$\pm$ 370	$\pm$ 350
750	[675, 770]	306	310	$\pm$15	$\pm$30	2 510	$\pm$ 170	$\pm$ 120
875	[790, 900]	166	144	$\pm$10	$\pm$16	1 020	$\pm$ 56	$\pm$ 23
1000	[900, 1025]	79	96	$\pm$ 9	$\pm$ 8	416	$\pm$ 25	$\pm$ 17
1125	[1010, 1155]	46	58	$\pm$ 7	$\pm$ 5	154	$\pm$ 8	$\pm$ 5
1250	[1120, 1280]	27	36	$\pm$ 5	$\pm$ 3	73	$\pm$ 4	$\pm$ 4
1275	[1145, 1305]	23	34	$\pm$ 5	$\pm$ 4	68.6	$\pm$ 3.3	$\pm$ 1.4
1375	[1235, 1410]	9	17	$\pm$ 3	$\pm$ 3	51.0	$\pm$ 2.0	$\pm$ 1.2
1500	[1345, 1535]	13	14	$\pm$ 3	$\pm$ 1.6	12.9	$\pm$ 0.8	$\pm$ 0.4
1625	[1455, 1665]	7	8.7	$\pm$ 2.6	$\pm$ 0.6	12.9	$\pm$ 0.8	$\pm$ 0.4
1750	[1565, 1790]	6	4.8	$\pm$ 2.0	$\pm$ 2.6	2.8	$\pm$ 0.1	$\pm$ 0.1
1875	[1680, 1920]	4	5.3	$\pm$ 2.2	$\pm$ 3.5	1.3	$\pm$ 0.1	$\pm$ 0.1
2000	[1790, ∞]	2	2.1	$\pm$ 1.2	$\pm$ 0.4	0.6	$\pm$ 0.1	$\pm$ 0.1
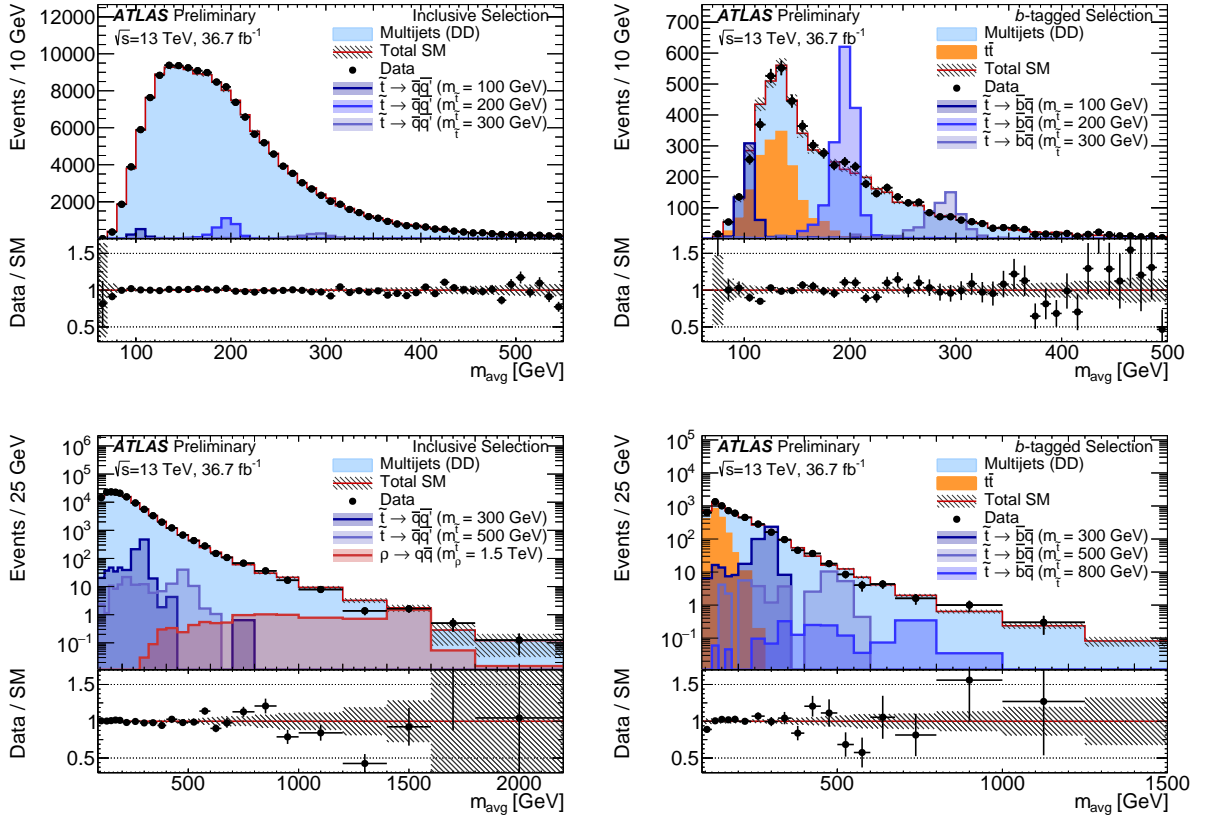
Figure 7: The m_{avg} spectrum in the signal region for the inclusive (left) and two-tag (right) selections shown in linear (top) and logarithmic scale (bottom). The data (black points) are compared to the total background prediction (red line) estimated with the data-driven method. The fraction of background coming from top-pair production is shown in orange. The statistical uncertainties of the prediction are shown in the grey hatched band. Signals of different masses are overlayed in different colours.


(a)   (b)
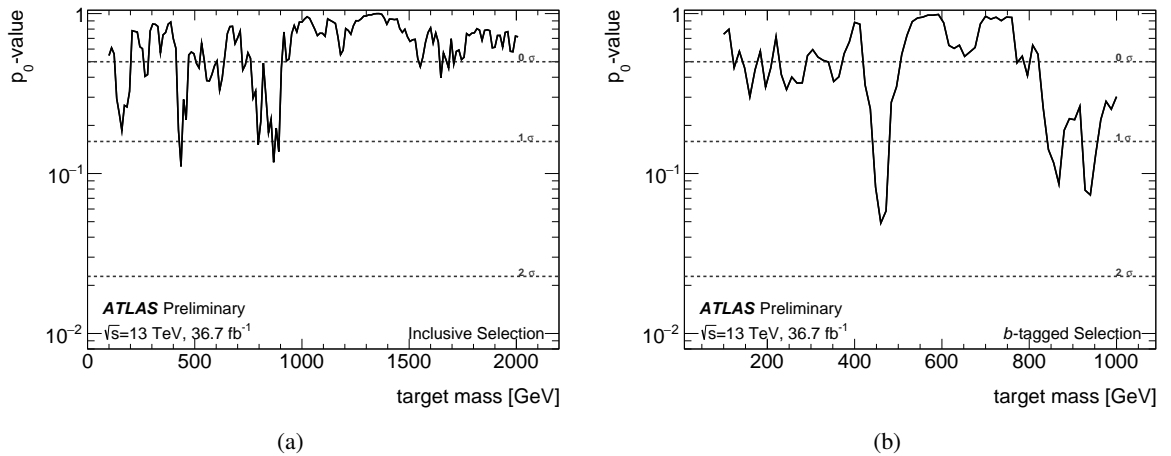
Figure 8: The observed local p_0-value (black line) in the inclusive (left) and two-tag (right) selections, shown as a function of the resonance mass hypothesis considered.

15

Table 5: The observed number of events in the data, N_{Data}, and the estimated number of background, N_{Bkg}, and expected signal, N_{Sig}, events with their statistical and systematic uncertainties computed in each mass window of the two-tag selection.

| $m_{\tilde{t}}$ [GeV]	Window [GeV]	N_{Data}	N_{Bkg} ($\pm$ stat. $\pm$ syst.)			N_{Sig} ($\pm$ stat. $\pm$ syst.)		
100	[100, 110]	256	285	±18	$\pm\ 51$	308	±18	$\pm\ 52$
125	[120, 135]	803	798	±28	±107	1 090	±40	±140
150	[140, 160]	809	789	±23	±132	1 510	±40	±130
175	[165, 185]	544	555	±16	$\pm\ 47$	1 300	±40	±140
200	[185, 210]	592	554	±13	$\pm\ 47$	1 220	±40	±110
225	[210, 235]	414	436	±11	$\pm\ 35$	893	±28	$\pm\ 90$
250	[230, 260]	416	385	±10	$\pm\ 32$	750	±60	±120
275	[255, 285]	302	283	$\pm\ 8$	$\pm\ 24$	480	±50	$\pm\ 60$
300	[275, 310]	242	250	$\pm\ 8$	$\pm\ 23$	390	±40	$\pm\ 50$
325	[300, 335]	181	179	$\pm\ 6$	$\pm\ 17$	273	±33	$\pm\ 34$
350	[320, 365]	169	161	$\pm\ 6$	$\pm\ 16$	225	±25	$\pm\ 20$
375	[345, 390]	110	111	$\pm\ 5$	$\pm\ 12$	147	±16	$\pm\ 22$
400	[365, 415]	80	96	$\pm\ 4$	$\pm\ 11$	114	$\pm\ 9$	$\pm\ 12$
425	[385, 440]	85	79	$\pm\ 4$	$\pm\ 10$	76	±14	$\pm\ 11$
450	[410, 465]	71	54.2	$\pm\ 3.0$	$\pm\ 7.1$	48	$\pm\ 9$	$\pm\ 10$
475	[430, 490]	67	46.8	$\pm\ 2.7$	$\pm\ 6.5$	40	$\pm\ 7$	$\pm\ 5$
500	[455, 515]	38	35.8	$\pm\ 2.3$	$\pm\ 5.3$	26	$\pm\ 5$	$\pm\ 5$
525	[475, 540]	31	35.1	$\pm\ 2.3$	$\pm\ 5.5$	21.7	$\pm\ 3.9$	$\pm\ 2.8$
550	[500, 565]	20	30.2	$\pm\ 2.1$	$\pm\ 5.0$	12.4	$\pm\ 2.5$	$\pm\ 2.3$
575	[520, 590]	14	26.3	$\pm\ 2.0$	$\pm\ 4.6$	17.5	$\pm\ 2.7$	$\pm\ 3.5$
600	[545, 620]	14	19.5	$\pm\ 1.6$	$\pm\ 3.5$	11.4	$\pm\ 0.9$	$\pm\ 1.5$
625	[565, 645]	15	15.8	$\pm\ 1.4$	$\pm\ 3.0$	9.3	$\pm\ 1.5$	$\pm\ 1.4$
650	[585, 670]	14	14.6	$\pm\ 1.3$	$\pm\ 2.9$	6.9	$\pm\ 1.2$	$\pm\ 1.1$
675	[610, 695]	13	13.6	$\pm\ 1.3$	$\pm\ 2.8$	5.5	$\pm\ 0.8$	$\pm\ 0.6$
700	[630, 720]	6	12.1	$\pm\ 1.2$	$\pm\ 2.6$	4.3	$\pm\ 0.6$	$\pm\ 0.5$
725	[655, 745]	5	9.9	$\pm\ 1.1$	$\pm\ 2.2$	4.4	$\pm\ 0.6$	$\pm\ 0.8$
750	[675, 770]	4	8.4	$\pm\ 0.1$	$\pm\ 1.9$	3.4	$\pm\ 0.5$	$\pm\ 0.5$
775	[700, 795]	8	6.9	$\pm\ 0.9$	$\pm\ 1.6$	2.4	$\pm\ 0.3$	$\pm\ 0.5$
800	[720, 820]	7	5.3	$\pm\ 0.7$	$\pm\ 1.3$	1.7	$\pm\ 0.3$	$\pm\ 0.2$

The observed and expected 95% CL upper limits on the allowed cross-sections are shown in Fig. 9. For top squarks decays into two quarks, the expected limit goes from 100 GeV to 430 GeV, with the observed limit excluding masses between 100 GeV and 410 GeV. If the top squark decay is into a *b*-quark and a light-quark, masses between 100 GeV and 530 GeV are expected to be excluded, with the observed exclusion ranging from 100 GeV to 470 GeV and from 480 GeV to 610 GeV. Pair-produced scalar gluons with decays into two gluons are excluded up to a mass of 800 GeV. Pair produced colorons coupling only to light quarks are excluded up to a mass of 1.5 TeV.
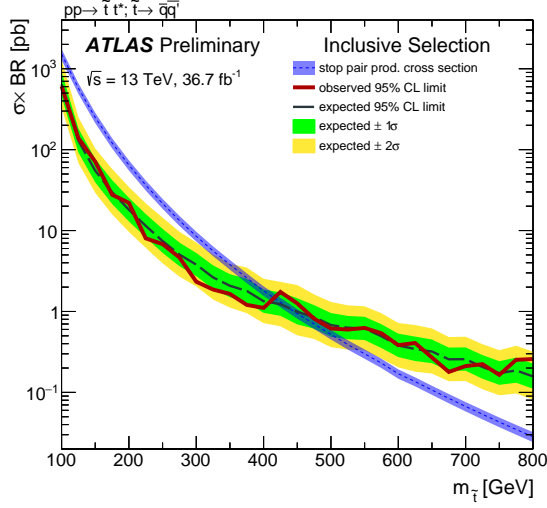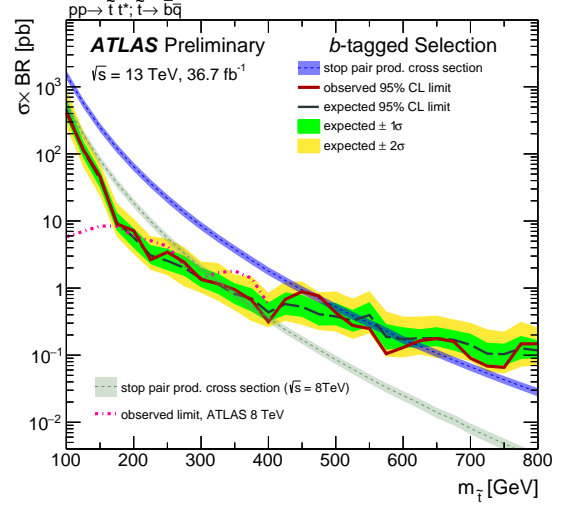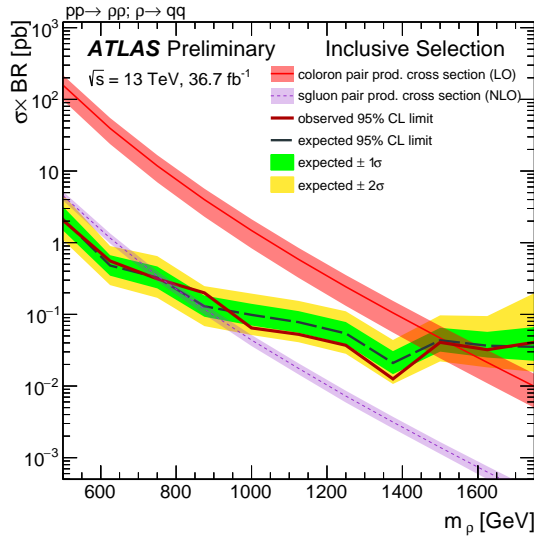
Figure 9: The 95% CL upper limit on the $\sigma \times BR$ compared to the theoretical cross-section for the direct pair-production of top squark with decays into (a) $\bar{q}\bar{q}'$ or (b) $\bar{b}\bar{s}$ and (c) high mass colorons decaying into qq and sgluons decaying into gg. The dashed black and solid red lines show the 95% CL expected and observed limits respectively, including all uncertainties except the theoretical signal cross-section uncertainty. The solid yellow (green) band around the expected limit shows the $\pm 1\sigma$ ($\pm 2\sigma$) uncertainties around this limit. The shaded coloured cross-section band indicates the $\pm 1\sigma$ variations due to theoretical uncertainties on the signal production cross-section given by renormalisation and factorisation scale and PDF uncertainties.

10 Conclusion

A search has been presented for the pair production of coloured resonances, each decaying into two jets. The analysis uses 36.7 fb^{-1} of pp collision data recorded in 2015 and 2016 by the ATLAS experiment at $\sqrt{s} = 13$ TeV. An inclusive selection and a selection with two b-tagged jets in the event are defined, and counting experiments are performed in windows of the average mass of the two resonance candidates. No significant deviation from the background prediction is observed. The results are interpreted in a SUSY simplified model with a top squark LSP which is pair-produced and decays promptly into two quarks through the λ'' R-parity violating couplings. For decays into two quarks top squark masses between $100\,\text{GeV} < m_{\tilde{t}} < 410\,\text{GeV}$ are excluded at 95% CL. If the top squark decays into a b-quark and a light-quark masses between $100\,\text{GeV} < m_{\tilde{t}} < 470\,\text{GeV}$ and $480\,\text{GeV} < m_{\tilde{t}} < 610\,\text{GeV}$ are excluded at 95% CL. Limits on the pair production of scalar gluons with decays into two-gluons reach masses of 800 GeV. Vector color octet resonances coupling only to light quarks are excluded up to masses of 1.5 TeV.

References

[1] Yu. A. Golfand and E. P. Likhtman,
Extension of the Algebra of Poincare Group Generators and Violation of p Invariance,
JETP Lett. **13** (1971) 323, [Pisma Zh. Eksp. Teor. Fiz.13,452(1971)].

[2] D. V. Volkov and V. P. Akulov, *Is the Neutrino a Goldstone Particle?*, Phys. Lett. **B46** (1973) 109.

[3] J. Wess and B. Zumino, *Supergauge Transformations in Four-Dimensions*,
Nucl. Phys. **B70** (1974) 39.

[4] J. Wess and B. Zumino, *Supergauge Invariant Extension of Quantum Electrodynamics*,
Nucl. Phys. **B78** (1974) 1.

[5] S. Ferrara and B. Zumino, *Supergauge Invariant Yang-Mills Theories*,
Nucl. Phys. **B79** (1974) 413.

[6] A. Salam and J. A. Strathdee, *Supersymmetry and Nonabelian Gauges*,
Phys. Lett. **B51** (1974) 353.

[7] G. R. Farrar and P. Fayet, *Phenomenology of the Production, Decay, and Detection of New Hadronic States Associated with Supersymmetry*, Phys. Lett. **B76** (1978) 575.

[8] R. Barbier et al., *R-parity violating supersymmetry*, Phys. Rept. **420** (2005) 1,
arXiv: `0406039 [hep-ph]`.

[9] H. K. Dreiner, *An Introduction to explicit R-parity violation*,
(1997), [Adv. Ser. Direct. High Energy Phys.21,565(2010)], arXiv: `9707435 [hep-ph]`.

[10] R. Barbieri and G. F. Giudice, *Upper Bounds on Supersymmetric Particle Masses*,
Nucl. Phys. **B306** (1988) 63.

[11] B. de Carlos and J. A. Casas, *One loop analysis of the electroweak breaking in supersymmetric models and the fine tuning problem*, Phys. Lett. **B309** (1993) 320, arXiv: `9303291 [hep-ph]`.

[12] K. Inoue, A. Kakuto, H. Komatsu and S. Takeshita,
Aspects of Grand Unified Models with Softly Broken Supersymmetry,
Prog. Theor. Phys. **68** (1982) 927, [Erratum: Prog. Theor. Phys.70,330(1983)].

[13] J. R. Ellis and S. Rudaz, *Search for Supersymmetry in Toponium Decays*,
Phys. Lett. **B128** (1983) 248.

[14] ATLAS Collaboration, *ATLAS Run 1 searches for direct pair production of third-generation squarks at the Large Hadron Collider*, Eur. Phys. J. **C75** (2015) 510,
arXiv: `1506.08616 [hep-ex]`.

[15] ATLAS Collaboration, *Search for top squarks in final states with one isolated lepton, jets, and missing transverse momentum in $\sqrt{s} = 13$ TeV pp collisions with the ATLAS detector*,
Phys. Rev. **D94** (2016) 052009, arXiv: `1606.03903 [hep-ex]`.

[16] CMS Collaboration, *Search for direct pair production of scalar top quarks in the single- and dilepton channels in proton–proton collisions at $\sqrt{s} = 8$ TeV*, JHEP **07** (2016) 027,
arXiv: `1602.03169 [hep-ex]`.

[17] CMS Collaboration, *Search for direct pair production of supersymmetric top quarks decaying to all-hadronic final states in pp collisions at $\sqrt{s} = 8$ TeV*, Eur. Phys. J. **C76** (2016) 460,
arXiv: `1603.00765 [hep-ex]`.

[18] CMS Collaboration, *Search for top squark pair production in compressed-mass-spectrum scenarios in proton–proton collisions at $\sqrt{s}$ = 8 TeV using the α_T variable*, Phys. Lett. **B767** (2017) 403, arXiv: 1605.08993 [hep-ex].

[19] CMS Collaboration, *Searches for pair production of third-generation squarks in $\sqrt{s}$ = 13 TeV pp collisions*, Submitted to Eur. Phys. J. C (2016), arXiv: 1612.03877 [hep-ex].

[20] CMS Collaboration, *Search for supersymmetry in the all-hadronic final state using top quark tagging in pp collisions at $\sqrt{s}$ = 13 TeV*, Submitted to Phys. Rev. D (2017), arXiv: 1701.01954 [hep-ex].

[21] B. C. Allanach, A. Dedes and H. K. Dreiner, *Bounds on R-parity violating couplings at the weak scale and at the GUT scale*, Phys. Rev. **D60** (1999) 075014, arXiv: 9906209 [hep-ph].

[22] G. D. Kribs, E. Poppitz and N. Weiner, *Flavor in supersymmetry with an extended R-symmetry*, Phys. Rev. **D78** (2008) 055010, arXiv: 0712.2039 [hep-ph].

[23] S. Y. Choi et al., *Color-Octet Scalars of N=2 Supersymmetry at the LHC*, Phys. Lett. **B672** (2009) 246, arXiv: 0812.3586 [hep-ph].

[24] S. Y. Choi, M. Drees, A. Freitas and P. M. Zerwas, *Testing the Majorana Nature of Gluinos and Neutralinos*, Phys. Rev. **D78** (2008) 095007, arXiv: 0808.2410 [hep-ph].

[25] T. Plehn and T. M. P. Tait, *Seeking Sgluons*, J. Phys. **G36** (2009) 075001, arXiv: 0810.3919 [hep-ph].

[26] C. Kilic, T. Okui and R. Sundrum, *Colored Resonances at the Tevatron: Phenomenology and Discovery Potential in Multijets*, JHEP **07** (2008) 038, arXiv: 0802.2568 [hep-ph].

[27] D. Alves, *Simplified Models for LHC New Physics Searches*, J. Phys. **G39** (2012) 105005, ed. by N. Arkani-Hamed et al., arXiv: 1105.2838 [hep-ph].

[28] P. H. Frampton and S. L. Glashow, *Chiral Color: An Alternative to the Standard Model*, Phys. Lett. **B190** (1987) 157.

[29] J. Bagger, C. Schmidt and S. King, *Axigluon Production in Hadronic Collisions*, Phys. Rev. **D37** (1988) 1188.

[30] C. T. Hill, *Topcolor: Top quark condensation in a gauge extension of the standard model*, Phys. Lett. **B266** (1991) 419.

[31] C. Kilic, T. Okui and R. Sundrum, *Vectorlike Confinement at the LHC*, JHEP **02** (2010) 018, arXiv: 0906.0577 [hep-ph].

[32] S. Schumann, A. Renaud and D. Zerwas, *Hadronically decaying color-adjoint scalars at the LHC*, JHEP **09** (2011) 074, arXiv: 1108.2957 [hep-ph].

[33] B. Lillie, L. Randall and L.-T. Wang, *The Bulk RS KK-gluon at the LHC*, JHEP **09** (2007) 074, arXiv: 0701166 [hep-ph].

[34] G. Burdman, B. A. Dobrescu and E. Ponton, *Resonances from two universal extra dimensions*, Phys. Rev. **D74** (2006) 075008, arXiv: 0601186 [hep-ph].

[35] ATLAS Collaboration, *Search for pair-produced massive coloured scalars in four-jet final states with the ATLAS detector in proton–proton collisions at $\sqrt{s}$ = 7 TeV*, Eur. Phys. J. **C73** (2013) 2263, arXiv: 1210.4826 [hep-ex].

[36] ATLAS Collaboration, *A search for top squarks with R-parity-violating decays to all-hadronic final states with the ATLAS detector in $\sqrt{s}$ = 8 TeV proton–proton collisions*, JHEP **06** (2016) 067, arXiv: 1601.07453 [hep-ex].

[37] CMS Collaboration, *Search for pair-produced dijet resonances in four-jet final states in pp collisions at $\sqrt{s}$ = 7 TeV*, Phys. Rev. Lett. **110** (2013) 141802, arXiv: 1302.0531 [hep-ex].

[38] CMS Collaboration, *Search for pair-produced resonances decaying to jet pairs in proton–proton collisions at $\sqrt{s}$ = 8 TeV*, Phys. Lett. **B747** (2015) 98, arXiv: 1412.7706 [hep-ex].

[39] ATLAS Collaboration, *Search for new phenomena in final states with large jet multiplicities and missing transverse momentum at $\sqrt{s}$ = 8 TeV proton–proton collisions using the ATLAS experiment*, JHEP **10** (2013) 130, arXiv: 1308.1841 [hep-ex].

[40] ATLAS Collaboration, *Search for supersymmetry at $\sqrt{s}$ = 8 TeV in final states with jets and two same-sign leptons or three leptons with the ATLAS detector*, JHEP **06** (2014) 035, arXiv: 1404.2500 [hep-ex].

[41] ATLAS Collaboration, *The ATLAS Experiment at the CERN Large Hadron Collider*, JINST **3** (2008) S08003.

[42] ATLAS Collaboration, *ATLAS Insertable B-Layer Technical Design Report*, (2010), URL: https://cds.cern.ch/record/1291633.

[43] ATLAS Collaboration, *Performance of the ATLAS Trigger System in 2015*, Submitted to Eur. Phys. J. C (2016), arXiv: 1611.09661 [hep-ex].

[44] ATLAS Collaboration, *Improved luminosity determination in pp collisions at $\sqrt{s}$ = 7 TeV using the ATLAS detector at the LHC*, Eur. Phys. J. **C73** (2013) 2518, arXiv: 1302.4393 [hep-ex].

[45] ATLAS Collaboration, *The ATLAS Simulation Infrastructure*, Eur. Phys. J. **C70** (2010) 823, arXiv: 1005.4568 [hep-ex].

[46] S. Agostinelli et al., *GEANT4: A Simulation toolkit*, Nucl. Instrum. Meth. **A506** (2003) 250.

[47] ATLAS Collaboration, *The simulation principle and performance of the ATLAS fast calorimeter simulation FastCaloSim*, ATL-PHYS-PUB-2010-013, 2010, URL: https://cds.cern.ch/record/1300517.

[48] T. Sjöstrand, S. Mrenna and P. Z. Skands, *A Brief Introduction to PYTHIA 8.1*, Comput. Phys. Commun. **178** (2008) 852, arXiv: 0710.3820 [hep-ph].

[49] ATLAS Collaboration, *Summary of ATLAS Pythia 8 tunes*, ATL-PHYS-PUB-2012-003, 2012, URL: https://cds.cern.ch/record/1474107.

[50] A. D. Martin, W. J. Stirling, R. S. Thorne and G. Watt, *Parton distributions for the LHC*, Eur. Phys. J. **C63** (2009) 189, arXiv: 0901.0002 [hep-ph].

[51] A. Sherstnev and R. S. Thorne, *Parton Distributions for LO Generators*, Eur. Phys. J. **C55** (2008) 553, arXiv: 0711.2473 [hep-ph].

[52] D. J. Lange, *The EvtGen particle decay simulation package*, Nucl. Instrum. Meth. **A462** (2001) 152.

[53] ATLAS Collaboration, *ATLAS Pythia 8 tunes to 7 TeV data*, ATL-PHYS-PUB-2014-021, 2014,
URL: https://cds.cern.ch/record/1966419.

[54] R. D. Ball et al., *Parton distributions with LHC data*, Nucl. Phys. **B867** (2013) 244,
arXiv: 1207.1303 [hep-ph].

[55] S. Alioli, P. Nason, C. Oleari and E. Re, *A general framework for implementing NLO calculations in shower Monte Carlo programs: the POWHEG BOX*, JHEP **06** (2010) 043,
arXiv: 1002.2581 [hep-ph].

[56] T. Sjostrand, S. Mrenna and P. Z. Skands, *PYTHIA 6.4 Physics and Manual*, JHEP **05** (2006) 026,
arXiv: 0603175 [hep-ph].

[57] P. Z. Skands, *Tuning Monte Carlo Generators: The Perugia Tunes*, Phys. Rev. **D82** (2010) 074018,
arXiv: 1005.3457 [hep-ph].

[58] M. Czakon and A. Mitov,
Top++: A Program for the Calculation of the Top-Pair Cross-Section at Hadron Colliders,
Comput. Phys. Commun. **185** (2014) 2930, arXiv: 1112.5675 [hep-ph].

[59] J. Alwall et al., *The automated computation of tree-level and next-to-leading order differential cross sections, and their matching to parton shower simulations*, JHEP **07** (2014) 079,
arXiv: 1405.0301 [hep-ph].

[60] L. Lönnblad and S. Prestel, *Merging Multi-leg NLO Matrix Elements with Parton Showers*,
JHEP **03** (2013) 166, arXiv: 1211.7278 [hep-ph].

[61] W. Beenakker, M. Kramer, T. Plehn, M. Spira and P. M. Zerwas,
Stop production at hadron colliders, Nucl. Phys. **B515** (1998) 3, arXiv: 9710451 [hep-ph].

[62] W. Beenakker et al., *Supersymmetric top and bottom squark production at hadron colliders*,
JHEP **08** (2010) 098, arXiv: 1006.4771 [hep-ph].

[63] W. Beenakker, S. Brensing, M. Kramer, A. Kulesza, E. Laenen et al.,
Squark and gluino hadroproduction, Int.J.Mod.Phys. **A26** (2011) 2637,
arXiv: 1105.1110 [hep-ph].

[64] C. Borschensky et al.,
Squark and gluino production cross sections in pp collisions at $\sqrt{s}$ = 13, 14, 33 and 100 TeV,
Eur. Phys. J. **C74** (2014) 3174, arXiv: 1407.5066 [hep-ph].

[65] M. Redi, V. Sanz, M. de Vries and A. Weiler, *Strong Signatures of Right-Handed Compositeness*,
JHEP **08** (2013) 008, arXiv: 1305.3818 [hep-ph].

[66] D. Goncalves-Netto, D. Lopez-Val, K. Mawatari, T. Plehn and I. Wigmore,
Sgluon Pair Production to Next-to-Leading Order, Phys. Rev. **D85** (2012) 114024,
arXiv: 1203.6358 [hep-ph].

[67] C. Degrande, B. Fuks, V. Hirschi, J. Proudom and H.-S. Shao, *Automated next-to-leading order predictions for new physics at the LHC: the case of colored scalar pair production*,
Phys. Rev. **D91** (2015) 094005, arXiv: 1412.5589 [hep-ph].

[68] W. Lampl et al., *Calorimeter Clustering Algorithms: Description and Performance*,
ATL-LARG-PUB-2008-002, 2008, URL: https://cds.cern.ch/record/1099735.

[69] M. Cacciari, G. P. Salam and G. Soyez, *The Anti-k_t jet clustering algorithm*, JHEP **04** (2008) 063,
arXiv: 0802.1189 [hep-ph].

[70] ATLAS Collaboration, *Jet energy scale and its systematic uncertainty in proton–proton collisions at $\sqrt{s}$ = 7 TeV with ATLAS 2011 data*, ATLAS-CONF-2013-004, 2013,
URL: https://cds.cern.ch/record/1509552.

[71] ATLAS Collaboration, *Determination of the jet energy scale and resolution at ATLAS using Z/γ-jet events in data at $\sqrt{s}$ = 8 TeV*, ATLAS-CONF-2015-057, 2015,
URL: https://cds.cern.ch/record/2059846.

[72] ATLAS Collaboration, *Jet Calibration and Systematic Uncertainties for Jets Reconstructed in the ATLAS Detector at $\sqrt{s}$ = 13 TeV*, ATL-PHYS-PUB-2015-015, 2015,
URL: https://cds.cern.ch/record/2037613.

[73] ATLAS Collaboration,
Selection of jets produced in 13 *TeV proton–proton collisions with the ATLAS detector*,
ATLAS-CONF-2015-029, 2015, URL: https://cds.cern.ch/record/2037702.

[74] ATLAS Collaboration, *Performance of b-Jet Identification in the ATLAS Experiment*,
JINST **11** (2016) P04008, arXiv: 1512.01094 [hep-ex].

[75] ATLAS Collaboration, *Optimisation of the ATLAS b-tagging performance for the 2016 LHC Run*,
ATL-PHYS-PUB-2016-012, 2016, URL: https://cds.cern.ch/record/2160731.

[76] E. A. Nadaraya, *On estimating regression*, Theory of Probability & Its Applications **9** (1964) 141.

[77] G. S. Watson, *Smooth regression analysis*,
Sankhyā: The Indian Journal of Statistics, Series A **26** (1964) 359,
URL: http://www.jstor.org/stable/25049340.

[78] ATLAS Collaboration, *Monte Carlo Calibration and Combination of In-situ Measurements of Jet Energy Scale, Jet Energy Resolution and Jet Mass in ATLAS*, ATLAS-CONF-2015-037, 2015,
URL: https://cds.cern.ch/record/2044941.

[79] G. Cowan, K. Cranmer, E. Gross and O. Vitells,
Asymptotic formulae for likelihood-based tests of new physics,
Eur. Phys. J. **C71** (2011) 1554, [Erratum: Eur. Phys. J.C73,2501(2013)],
arXiv: 1007.1727 [physics.data-an].

[80] A. L. Read, *Presentation of search results: The CL(s) technique*, J. Phys. **G28** (2002) 2693.

[81] M. Baak et al., *HistFitter software framework for statistical data analysis*,
Eur. Phys. J. **C75** (2015) 153, arXiv: 1410.1280 [hep-ex].